

Relating CNN-Transformer Fusion Network for Change Detection

Yuhao Gao, Gensheng Pei, Mengmeng Sheng, Zeren Sun, Tao Chen and Yazhou Yao
School of Computer Science and Engineering, Nanjing University of Science and Technology, Nanjing, China
{yuhao_0, peigsh, shengmengmeng, zere ns, taochen, yazhou.yao}@njjust.edu.cn

Abstract—While deep learning, particularly convolutional neural networks (CNNs), has revolutionized remote sensing (RS) change detection (CD), existing approaches often miss crucial features due to neglecting global context and incomplete change learning. Additionally, transformer networks struggle with low-level details. RCTNet addresses these limitations by introducing (1) an early fusion backbone to exploit both spatial and temporal features early on, (2) a Cross-Stage Aggregation (CSA) module for enhanced temporal representation, (3) a Multi-Scale Feature Fusion (MSF) module for enriched feature extraction in the decoder, and (4) an Efficient Self-deciphering Attention (ESA) module utilizing transformers to capture global information and fine-grained details for accurate change detection. Extensive experiments demonstrate RCTNet’s clear superiority over traditional RS image CD methods, showing significant improvement and an optimal balance between accuracy and computational cost. Our source codes and pre-trained models are available at: <https://github.com/NUST-Machine-Intelligence-Laboratory/RCTNet>.

Index Terms—Change Detection, Cross-Stage Aggregation, Multi-Scale Fusion

I. INTRODUCTION

Change detection (CD) in remote sensing (RS) images stands as a critical technique for identifying semantic changes like building development or land cover modifications across geographically identical areas captured at different times. Its applications are extensive applications support diverse fields like damage assessment, urban planning, and natural disaster monitoring. RS images often encompass complex backgrounds and are susceptible to lighting variations. Fig. 1 illustrates the challenges faced by the existing remote sensing change detection. To address these challenges, researchers have employed a variety of techniques. Early CD methods relied on algorithms like Change Vector Analysis (CVA), Support Vector Machines (SVM), Kauth-Thomas (KT), and Principal Component Analysis (PCA), which demanded complex feature engineering and faced limitations in generalizability.

Modern solutions have embraced the power of Convolutional Neural Networks (CNNs) for RS image CD tasks. Daudt *et al.* [1] pioneer U-Net-inspired Siamese Fully Convolutional Networks (FCNs) for CD, establishing a foundational framework with its investigation of skip connection strategies. Hafner *et al.* [2] utilize a dual-stream U-Net for data fusion from Sentinel-1 and Sentinel-2 images, while DASNet [3] incorporates the extended attention mechanism for enhancing building change detection. However, these approaches with expanded receptive fields often encounter a trade-off between global representation and computational complexity inherent

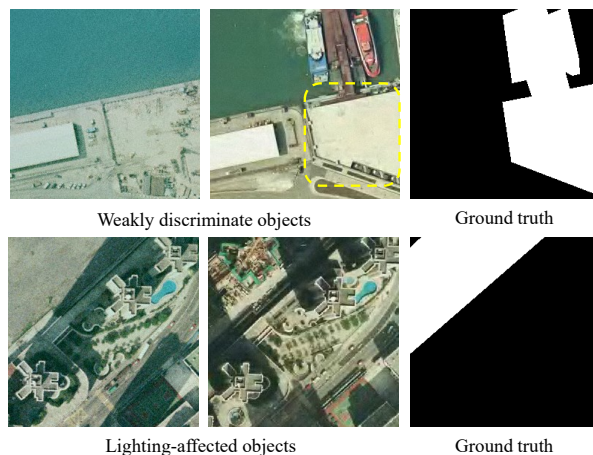


Fig. 1. The illustration of challenging scenarios, *e.g.*, weakly discriminate objects and lighting-affected objects. The characteristics of the labeled building presented in the first example are similar to that of the ground. The second example shows shadow interference in changed regions.

to CNNs. This spurs explorations into Transformers [4], renowned for their exceptional ability to model global information relationships. The technology, previously reserved for natural language processing, has seen rapid advancements in vision tasks, *e.g.*, image classification [5]–[11], object detection [12]–[14], and segmentation [15]–[24]. This led to the integration of Transformers in bitemporal RS image CD, with SwinSUNet [25] attempting the pure transformer but encountering computational challenges. Chen *et al.* [26] propose the Bitemporal Image Transformer (BIT) method, combining CNN and transformers for feature extraction, yet its single-scale nature limits performance in subtle change regions. Bandara *et al.* [27] address this with a hierarchical transformer encoder coupled with a lightweight MLP decoder, effectively exploiting multi-layer features but with less efficient spatiotemporal detail correlation.

Motivated by the complementary nature of high-level semantic information and low-level detailed features crucial for change detection, we propose RCTNet, a hybrid network integrating the strengths of CNNs and Transformers. At its core lies the Cross-Stage Aggregation (CSA) module, which fuses features from different backbone stages. This fusion enriches both semantic information and fine-grained details of objects, empowering the model to capture the broader context and the intricate nuances within the image. An element-wise subtrac-

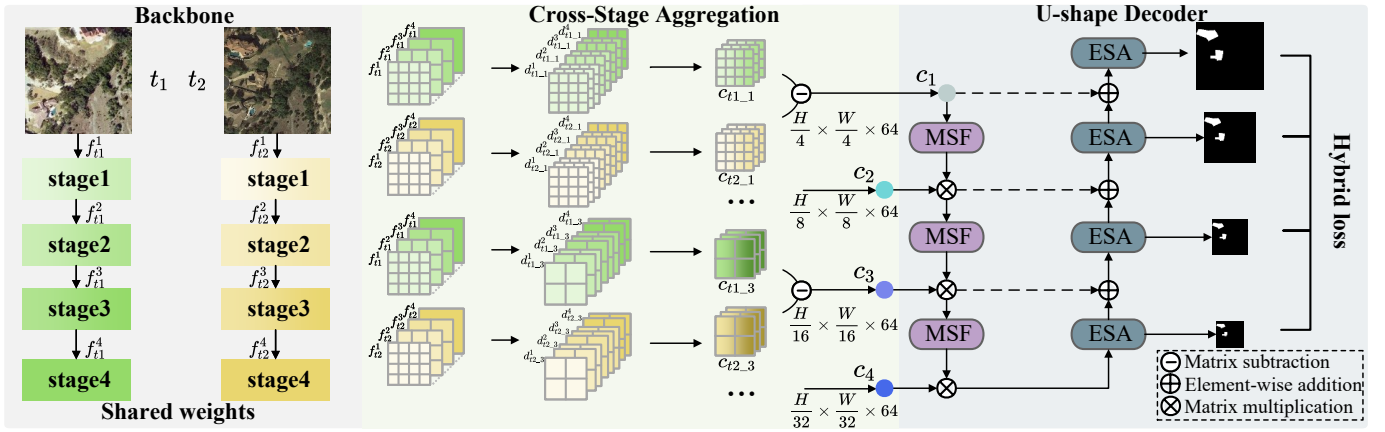


Fig. 2. An illustration of our RCTNet. Our proposed architecture comprises three key modules: a shared-weight backbone for temporal feature extraction, a Cross-Stage Aggregation (CSA, §II-B) module for enhanced representation at each stage, and a U-shape decoder utilizing Multi-Scale Fusion (MSF, §II-C) and Efficient Self-deciphering Attention (ESA, §II-C) for robust decoding. RegNet extracts features from a registered image pair, and the CSA module enriches each stage’s output. Finally, the U-shape decoder fuses multi-scale features through MSF and leverages ESA for accurate predictions.

tion followed by an absolute value operation then computes temporal difference features, highlighting changes between the bitemporal images. These aggregated and enriched features are subsequently fed into the lightweight U-shape decoder. This decoder contains two core modules: Multi-Scale Feature Fusion (MSF) and Efficient Self-deciphering Attention (ESA). MSF further enhances the expressive capacity of the features by extracting information at multiple scales. At the same time, ESA incorporates global semantic relationships into each decoder layer, allowing the model to capture complex object changes effectively and ultimately boosting accuracy. Our contributions can be summarized as follows:

- (1) We introduce a new CSA module that seamlessly integrates features from diverse stages of the backbone network. This fusion enriches both semantic information and fine-grained details across high-level and low-level feature maps, empowering the model to capture both context and intricate changes.
- (2) We develop a lightweight U-shape decoder comprising two core modules: MSF and ESA. MSF improves semantic relationships between output features across different levels via multi-scale feature extraction, while ESA focuses on enhancing feature accuracy by computing global semantic relationships at each layer.
- (3) We rigorously evaluate RCTNet on three representative CD datasets. Compared to existing state-of-the-art models, RCTNet achieves superior or highly competitive performance across all benchmark datasets, demonstrating its exceptional effectiveness in change detection tasks.

II. METHODOLOGY

A. Overview

Fig. 2 depicts the overall architecture of RCTNet. The input bitemporal images, t_1 and t_2 , of size $H \times W \times 3$ are fed into a shared-weight Siamese network to extract features. RCTNet downsamples the images through four stages, each

containing a convolutional layer with stride 2. This progressive downsampling enables the network to learn semantic features at different scales, enhancing training stability. Each stage also utilizes max pooling for downsampling and feature preservation, facilitating the extraction of higher-level features.

RCTNet employs the lightweight RegNet [28] for feature extraction. Our proposed Cross-Stage Aggregation (CSA) module fuses features from different backbone stages, enriching semantic information and fine-grained details across feature maps. A lightweight U-shape decoder with two core modules further refines the extracted features. Multi-Scale Feature Fusion (MSF) enhances semantic relationships by extracting multi-scale features, while Efficient Self-deciphering Attention (ESA) incorporates global semantic connections into each decoder layer, ultimately boosting model accuracy.

B. Cross-Stage Aggregation

The Cross-Stage Aggregation (CSA) module comprises four parallel branches, each processing features extracted from different stages of the backbone for the corresponding bitemporal image. Focusing on the second branch (see Fig. 3), we illustrate how it transforms feature maps $f_{t1}^1, f_{t1}^2, f_{t1}^3, f_{t1}^4$ (extracted from stages $i = 1, 2$ of image t_i) into the output feature map $c_{t1,2}$. To align spatial resolutions, f_{t1}^1 undergoes max pooling and a 3×3 convolutional layer with channel adjustment. Similarly, f_{t1}^2 receives a 3×3 convolutional layer for channel matching. Features f_{t1}^3 and f_{t1}^4 are downsampled using bilinear upsampling and 3×3 convolutional layers for channel reduction, aligning them with the intermediate resolution. Finally, all aligned feature maps are concatenated and processed by a final 3×3 convolutional layer with batch normalization and ReLU activation, generating the output $c_{t1,2}$.

The CSA module carefully balances feature quantity and detail by allocating the following channel numbers to the four branches: 32, 64, 32, and 16. This configuration retains high-resolution features from shallower layers (32 channels) while

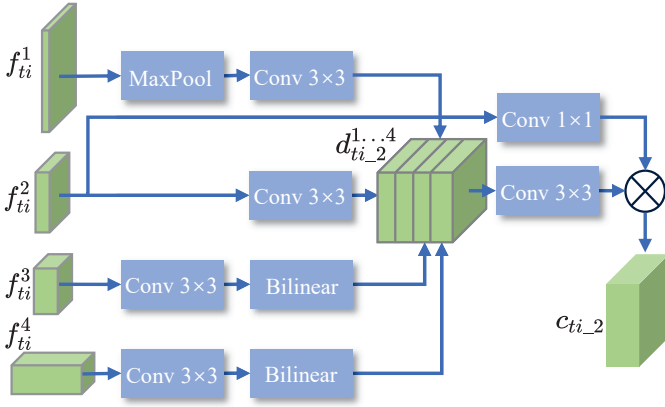


Fig. 3. Illustration of cross-stage aggregation (CSA).

incorporating semantic information from deeper layers (64 channels). In effect, the module leverages both details and context to enrich the aggregated representation. The complete feature transformation process can be summarized as:

$$\begin{aligned}
 d_{ti,2}^1 &= \text{Conv}_{3 \times 3} (\text{Maxpool} (f_{ti}^1)) \in \mathbb{R}^{H/8 \times W/8 \times 64}, \\
 d_{ti,2}^2 &= \text{Conv}_{3 \times 3} (f_{ti}^2) \in \mathbb{R}^{H/8 \times W/8 \times 64}, \\
 d_{ti,2}^3 &= \text{Up} (\text{Conv}_{3 \times 3} (f_{ti}^3)) \in \mathbb{R}^{H/8 \times W/8 \times 64}, \\
 d_{ti,2}^4 &= \text{Up} (\text{Up} (\text{Conv}_{3 \times 3} (f_{ti}^4))) \in \mathbb{R}^{H/8 \times W/8 \times 64}.
 \end{aligned} \quad (1)$$

Here, $\text{Maxpool}(\cdot)$ represents the max-pooling operation, and $\text{Up}(\cdot)$ denotes bilinear upsampling. Each $d_{ti,2}^i$ is a feature map extracted from the i -th stage of the backbone network for image t_i . These features are then combined through concatenation to capture richer spatial context information.

Following the feature transformation in the CSA branches, we further refine both f_{ti}^2 and the concatenated features. A 1×1 convolutional layer projects f_{ti}^2 to a consistent embedding dimension, while a 3×3 convolutional layer transforms the concatenated features. These processed representations then undergo a matrix multiplication operation, enabling the fusion of global and local information captured by the different components, formalized as:

$$c_{ti,2} = f_{ti}^2' \otimes \text{Conv}_{3 \times 3} (\text{Cat} (d_{ti,2}^1, d_{ti,2}^2, d_{ti,2}^3, d_{ti,2}^4)), \quad (2)$$

where \otimes indicates matrix multiplication, and Cat denotes feature concatenation. $c_{ti,2}$ is the final output feature map, and f_{ti}^2' is the transformed f_{ti}^2 . Similar operations are performed for the other CSA branches, enabling information integration across different spatial scales and semantic levels.

C. Paying Attention to Multi-Scale Features

Multi-Scale Fusion. Seeking to enhance the capture of temporal change information, we introduce the Multi-Scale Fusion (MSF) module, leveraging a series of convolution operations. As depicted in Fig. 4 (a), MSF branches into four paths, each applying a convolution to the previous base feature map. These

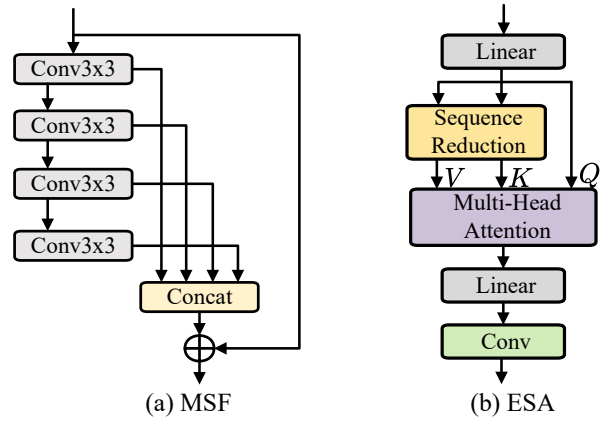


Fig. 4. Illustration of the two modules in U-shape decoder.

branches extract features at distinct scales, thereby enriching the final representation via concatenation.

$$\begin{aligned}
 c' &= \text{Conv}_{3 \times 3} (c_{in}), c'' = \text{Conv}_{3 \times 3} (c'), \\
 c''' &= \text{Conv}_{3 \times 3} (c''), c'''' = \text{Conv}_{3 \times 3} (c'''), \\
 c_{out} &= c_{in} \oplus \text{Cat} (c', c'', c''', c''').
 \end{aligned} \quad (3)$$

Further, we incorporate residual learning to preserve salient information and yield more expressive image features.

Efficient Self-deciphering Attention. While the U-shape network architecture effectively combines multi-level features, its output lacks global semantic context, limiting CD accuracy. Inspired by SegFormer [38], we introduce the Efficient Self-deciphering Attention (ESA) module to integrate global semantic relationships across decoder layers. Fig. 4 (b) illustrates ESA, which resembles a standard self-attention structure but adopts sequence reduction for computational efficiency. Assuming each of the heads Q, K, V have the same dimensions $N \times C$, N vectors each of dimension C , the self-attention is represented as:

$$\text{Attention}(Q, K, V) = \text{Softmax} \left(\frac{QK^T}{\sqrt{d_{\text{head}}}} \right) V. \quad (4)$$

Traditionally, self-attention exhibits $\mathcal{O}(N^2)$ time complexity, where N denotes the sequence length. To address this, ESA leverages sequence reduction with a reduction ratio R . This involves two steps: firstly, reshaping the key matrix K from $N \times C$ to $\frac{N}{R} \times (C \cdot R)$ while preserving information. Secondly, a linear layer projects the reshaped matrix back to its original dimensions $\frac{N}{R} \times C$. Similar operations are applied to the value matrix V . Consequently, the time complexity reduces to $\mathcal{O}\left(\frac{N^2}{R}\right)$, significantly improving efficiency. In our experiments, we set R to 4 for all decoder stages.

D. Loss Function

This paper utilizes a hybrid loss function to enhance training by combining the strengths of binary cross-entropy (BCE) and Dice losses. Our loss function is defined as:

$$\mathcal{L} = \mathcal{L}_{\text{bce}} + \mathcal{L}_{\text{dice}}. \quad (5)$$

TABLE I
QUANTITATIVE COMPARISONS ON THE WHU-CD [29], LEVIR-CD [30] AND SYSU-CD [31] DATASETS. THE BEST TWO RESULTS ARE HIGHLIGHTED IN RED AND BLUE. ALL RESULTS ARE DESCRIBED AS PERCENTAGES (%).

Method	Backbone	WHU-CD				LEVIR-CD				SYSU-CD			
		F1	P	R	IoU	F1	P	R	IoU	F1	P	R	IoU
FC-EF ₁₈ [1]	VGG	72.01	77.69	67.10	56.26	83.4	86.91	80.17	71.53	75.07	74.32	75.84	60.09
FC-Siam-diff ₁₈ [1]	VGG	58.81	47.33	77.66	41.66	86.31	89.53	83.31	75.92	72.57	89.13	61.21	56.96
FC-Siam-conc ₁₈ [1]	VGG	66.63	60.88	73.58	49.95	83.69	91.99	76.77	71.96	76.35	82.54	71.03	61.75
IFNet ₂₀ [32]	VGG	83.11	92.24	75.78	71.12	88.13	91.78	82.93	78.77	76.38	82.44	72.38	61.85
BIT ₂₂ [26]	ResNet18	83.98	86.64	81.48	72.39	89.31	89.24	89.37	80.68	79.40	82.32	76.68	65.84
SNUNet ₂₂ [33]	UNet++	83.50	85.60	81.49	71.67	88.16	89.18	87.17	78.83	79.96	81.95	78.08	66.62
ChangeFormer ₂₂ [27]	ViT	89.88	91.83	88.02	81.63	90.40	92.05	88.80	82.48	77.83	81.30	74.65	63.71
TinyCD ₂₃ [34]	EfficientNet	91.48	92.22	90.74	84.30	91.05	92.68	89.47	83.57	80.96	85.71	76.71	68.01
DGANet ₂₃ [14]	CNN	90.87	95.59	86.59	83.27	90.26	92.03	88.56	82.25	79.79	78.86	80.74	66.37
HSSENet ₂₃ [35]	ResNet18	91.55	94.56	88.73	84.42	91.48	92.63	90.35	84.29	-	-	-	-
WNet ₂₃ [36]	ResNet18	91.25	92.37	90.15	83.91	90.67	91.16	90.18	82.93	80.64	81.71	79.58	67.55
TransY-Net ₂₃ [37]	Swin Transformer	93.38	94.68	92.12	87.58	91.90	92.90	89.35	83.64	82.84	89.09	77.42	70.71
RCTNet (Ours)	ResNet18	94.11	95.84	92.43	88.87	91.33	92.75	89.95	84.04	82.23	85.62	79.10	69.83
	RegNet	95.05	96.04	94.09	90.57	91.93	92.91	90.97	85.07	83.01	84.33	81.73	70.96

The \mathcal{L}_{bce} focuses on pixel-level classification accuracy and is formulated as:

$$\mathcal{L}_{\text{bce}}(p, g) = g \cdot \log(p) + (1 - g) \cdot \log(1 - p), \quad (6)$$

where p is the predicted change map, g is the corresponding ground truth, and \cdot denotes element-wise product. The Dice loss emphasizes spatial overlap between predictions and ground truth, calculated as:

$$\mathcal{L}_{\text{dice}}(p, g) = 1 - \frac{2 \cdot p \cdot g}{\|p\|_1 + \|g\|_1}, \quad (7)$$

where $\|\cdot\|_1$ denotes the ℓ_1 norm. For our multi-stage predictions, the total loss is computed by summing the individual losses across all stages:

$$\mathcal{L}(p, g) = \sum_{i=1}^4 \mathcal{L}_{\text{bce}}(p_i, g) + \sum_{i=1}^4 \mathcal{L}_{\text{dice}}(p_i, g), \quad (8)$$

where p_i represents the predicted change map for stage i .

III. EXPERIMENTS

A. Experimental Setup

Datasets. In this work, we evaluate our RCTNet on three challenging change detection benchmarks: WHU-CD [29], LEVIR-CD [30], and SYSU-CD [31]. LEVIR-CD comprises 637 image pairs at 1024×1024 resolution, WHU-CD consists of a single image pair at a larger size of 32507×15354 , and SYSU-CD provides a substantial collection of 20,000 image patches (256×256 , 0.5m resolution) for CD tasks.

Evaluation Metrics. To comprehensively evaluate the performance of our approach, we calculate four key metrics: Precision (P), Recall (R), F1-score (F1), and Intersection over Union (IoU). These metrics are defined as follows:

$$\begin{aligned} P &= \frac{TP}{TP + FP}, & R &= \frac{TP}{TP + FN}, \\ F1 &= \frac{2 \times P \times R}{P + R}, & \text{IoU} &= \frac{TP}{FN + FP + TP}, \end{aligned} \quad (9)$$

TABLE II
COMPARISON RESULTS OF THE NUMBER OF PARAMETERS (PARAMS, M) AND COMPUTATIONAL COST (FLOPS, G). THE BEST RESULT IS HIGHLIGHTED IN RED.

Method	Params	FLOPs	WHU-CD	LEVIR-CD	SYSU-CD
IFNet ₂₀ [32]	50.71	82.26	83.11	88.13	76.38
SNUNet ₂₂ [33]	12.03	42.96	83.50	88.16	79.96
ChangeFormer ₂₂ [27]	41.02	202.87	89.88	90.40	77.83
DGANet ₂₃ [14]	12.28	12.56	90.87	90.26	79.79
WNet ₂₃ [36]	43.07	19.20	91.25	90.67	80.64
RCTNet (ResNet18)	14.6	8.43	94.11	91.33	82.23
RCTNet (RegNet)	13.8	7.65	95.05	91.93	83.01

where TP, TN, FP, and FN represent true positives, true negatives, false positives, and false negatives, respectively.

Implementation Details. Our RCTNet implementation uses the PyTorch libraries [39] and utilizes an NVIDIA V100 GPU for training and testing. The network backbone is initialized with pre-trained weights from the RegNetY-1.6GF model [28] trained on ImageNet. We employ the Adam optimizer [40] with a momentum of 0.9, weight decay of 0.0001, and parameters β_1 and β_2 set to 0.9 and 0.99, respectively. The initial learning rate is 0.0005 and is dynamically adjusted during training using a poly learning rate decay with a power of 0.9. We train with a batch size of 32 for 50,000 iterations. Following previous works [1], [27], [33], [34], we divide the images in these datasets into patches of size 256×256 . We apply random flipping, cropping, and temporal exchange to augment the training data to the input images.

B. State-of-the-art Comparisons

To comprehensively evaluate the effectiveness and efficiency of our proposed RCTNet for the change detection task

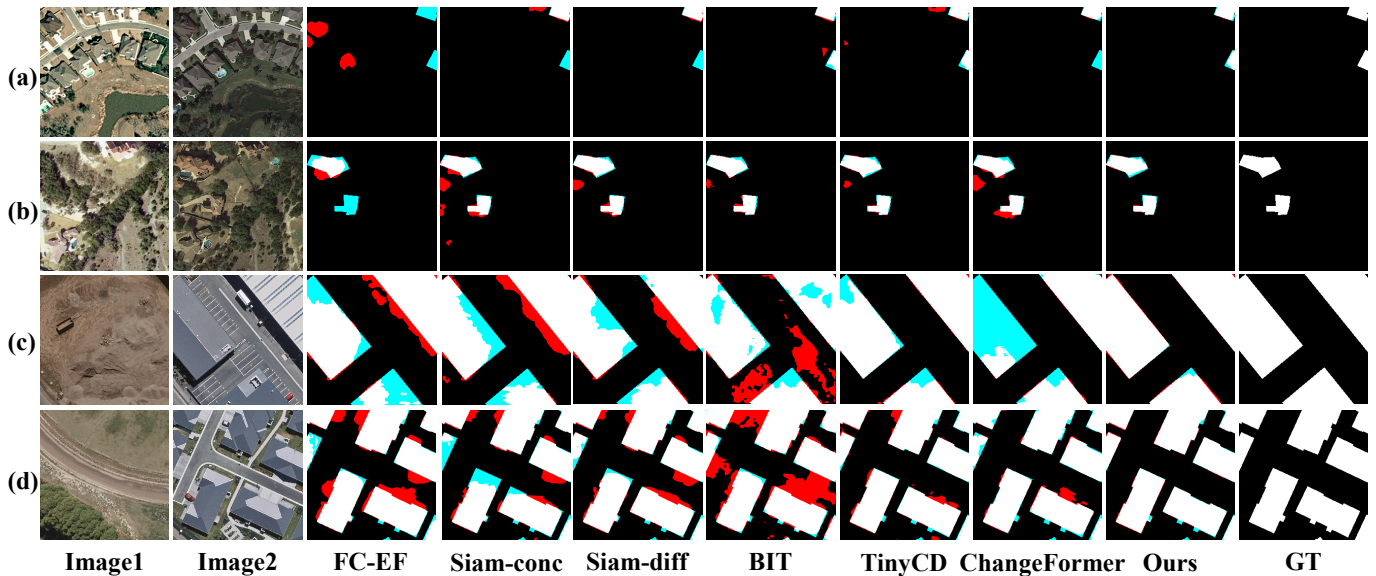


Fig. 5. Qualitative comparisons of our proposed method and state-of-the-art approaches on two benchmark datasets, LEVIR-CD [30] and WHU-CD [29]. Examples (a) and (b) showcase results on LEVIR-CD, while (c) and (d) focus on WHU-CD. In each sample, “GT” represents the ground truth, white areas denote true positives, black areas represent true negatives, red areas indicate false positives, and blue areas represent false negatives.

on bitemporal remote sensing images, we benchmark it against several state-of-the-art approaches [1], [14], [26], [27], [32]–[37].

Quantitative Results. Compared to several state-of-the-art change detection approaches, our RCTNet surpasses them on benchmark datasets, as evidenced by Table I. RCTNet performs best in F1 and IoU metrics compared to existing methods. In particular, for the WHU-CD dataset, our RCTNet (*w/* RegNet) improves by **1.67** and **2.99** in terms of F1 and IoU metrics. Furthermore, as depicted in Table II, RCTNet showcases competitive computational efficiency while maintaining strong performance, featuring less number of parameters (Params) and floating point operations (FLOPs).

Qualitative Results. Fig. 5 presents visual comparisons of our method and other approaches on the LEVIR-CD and WHU-CD datasets. The presented approach skillfully retains the integrity of change information while preserving edge details through the effective extraction of the large-area and small-area change information. Compared to previous methods, the proposed method demonstrates the capability to achieve relatively comprehensive detection results.

C. Ablation Studies

In this section, we conduct a series of ablation experiments on the LEVIR-CD validation set to scrutinize the effectiveness of the proposed components with RCTNet (*w/* RegNet). Table III illustrates that the ablated versions of individual components exhibit varying degrees of performance degradation in comparison to the full model. The ablation results demonstrate the effectiveness of our proposed modules. Our introduction of RCTNet seamlessly merges features from various backbone network stages, enhancing semantic information and fine-grained details in multi-level feature maps.

TABLE III
ABLATION STUDIES OF THE PROPOSED THREE KEY COMPONENTS ON LEVIR-CD [30]. THE BEST RESULT IS HIGHLIGHTED IN RED.

#	Component	F1	P	R	IoU
1	<i>w/o</i> CSA	91.52	92.55	90.50	84.36
2	<i>w/o</i> MSF	91.84	92.78	90.92	84.91
3	<i>w/o</i> ESA	91.67	92.86	90.52	84.63
4	Full (Ours)	91.93	92.91	90.97	85.07

IV. CONCLUSION

Our proposed deep learning approach, RCTNet, alleviates the limitations of existing change detection methods by mitigating inaccuracies from atmospheric variations, lighting changes, and phenological shifts. This impressive effort is achieved through a synergistic combination of the convolutional neural network and Transformer strengths. Rigorous experimentation across diverse datasets demonstrates RCTNet’s clear superiority over state-of-the-art models. It exhibits substantial accuracy improvements and a favorable trade-off between performance and computational cost.

REFERENCES

- [1] R. C. Daudt, B. Le Saux, and A. Boulch, “Fully convolutional siamese networks for change detection,” in *IEEE International Conference on Image Processing*, 2018, pp. 4063–4067.
- [2] S. Hafner, A. Nascetti, H. Azizpour, and Y. Ban, “Sentinel-1 and sentinel-2 data fusion for urban change detection using a dual stream u-net,” *IEEE Geoscience and Remote Sensing Letters*, vol. 19, pp. 1–5, 2021.
- [3] J. Chen, Z. Yuan, J. Peng, L. Chen, H. Huang, J. Zhu, Y. Liu, and H. Li, “Dasnet: Dual attentive fully convolutional siamese networks for change detection in high-resolution satellite images,” *IEEE Journal of Selected*

- Topics in Applied Earth Observations and Remote Sensing*, vol. 14, pp. 1194–1206, 2020.
- [4] A. Dosovitskiy, L. Beyer, A. Kolesnikov, D. Weissenborn, X. Zhai, T. Unterthiner, M. Dehghani, M. Minderer, G. Heigold, S. Gelly, J. Uszkoreit, and N. Houlsby, “An image is worth 16x16 words: Transformers for image recognition at scale,” in *International Conference on Learning Representations*, 2021, pp. 1–22.
 - [5] Yazhou Yao, Jian Zhang, Fumin Shen, Li Liu, Fan Zhu, Dongxiang Zhang, and Heng Tao Shen, “Towards automatic construction of diverse, high-quality image datasets,” *IEEE Transactions on Knowledge and Data Engineering*, vol. 32, no. 6, pp. 1199–1211, 2020.
 - [6] Yazhou Yao, Zeren Sun, Chuanyi Zhang, Fumin Shen, Qi Wu, Jian Zhang, and Zhenmin Tang, “Jo-src: A contrastive approach for combating noisy labels,” in *IEEE Conference on Computer Vision and Pattern Recognition*, 2021, pp. 5192–5201.
 - [7] Zeren Sun, Yazhou Yao, Xiu-Shen Wei, Yongshun Zhang, Fumin Shen, Jianxin Wu, Jian Zhang, and Heng Tao Shen, “Webly supervised fine-grained recognition: Benchmark datasets and an approach,” in *IEEE International Conference on Computer Vision*, 2021, pp. 10602–10611.
 - [8] Yazhou Yao, Jian Zhang, Fumin Shen, Xiansheng Hua, Jingsong Xu, and Zhenmin Tang, “Exploiting web images for dataset construction: A domain robust approach,” *IEEE Transactions on Multimedia*, vol. 19, no. 8, pp. 1771–1784, 2017.
 - [9] Mengmeng Sheng, Zeren Sun, Zhenhuang Cai, Tao Chen, Yichao Zhou, and Yazhou Yao, “Adaptive integration of partial label learning and negative learning for enhanced noisy label learning,” in *AAAI*, 2024, pp. 4820–4828.
 - [10] Zeren Sun, Fumin Shen, Dan Huang, Qiong Wang, Xiangbo Shu, Yazhou Yao, and Jinhui Tang, “Pnp: Robust learning from noisy labels by probabilistic noise prediction,” in *IEEE Conference on Computer Vision and Pattern Recognition*, 2022, pp. 5311–5320.
 - [11] Huafeng Liu, Chuanyi Zhang, Yazhou Yao, Xiu-Shen Wei, Fumin Shen, Zhenmin Tang, and Jian Zhang, “Exploiting web images for fine-grained visual recognition by eliminating open-set noise and utilizing hard examples,” *IEEE Transactions on Multimedia*, vol. 24, pp. 546–557, 2022.
 - [12] Yazhou Yao, Tao Chen, Hanbo Bi, Xinhao Cai, Gensheng Pei, Guoye Yang, Zhiyuan Yan, Xian Sun, Xing Xu, and Hai Zhang, “Automated object recognition in high-resolution optical remote sensing imagery,” *National Science Review*, vol. 10, no. 6, pp. nwad122, 2023.
 - [13] Xinhao Cai, Qiuxia Lai, Yuwei Wang, Wenguan Wang, Zeren Sun, and Yazhou Yao, “Poly kernel inception network for remote sensing detection,” in *IEEE Conference on Computer Vision and Pattern Recognition*, 2024, pp. 27706–27716.
 - [14] M. Zhang, Q. Li, Y. Miao, Y. Yuan, and Q. Wang, “Difference-guided aggregation network with multi-image pixel contrast for change detection,” *IEEE Transactions on Geoscience and Remote Sensing*, vol. 61, pp. 1–14, 2023.
 - [15] G. Pei, F. Shen, Y. Yao, G. Xie, Z. Tang, and J. Tang, “Hierarchical feature alignment network for unsupervised video object segmentation,” in *European Conference on Computer Vision*, 2022, pp. 596–613.
 - [16] H. Liu, P. Peng, T. Chen, Q. Wang, Y. Yao, and X. Hua, “Fecanet: Boosting few-shot semantic segmentation with feature-enhanced context-aware network,” *IEEE Transactions on Multimedia*, vol. 25, pp. 8580–8592, 2023.
 - [17] Y. Yao, T. Chen, G. Xie, C. Zhang, F. Shen, Q. Wu, Z. Tang, and J. Zhang, “Non-salient region object mining for weakly supervised semantic segmentation,” in *IEEE Conference on Computer Vision and Pattern Recognition*, 2021, pp. 2623–2632.
 - [18] Gensheng Pei, Fumin Shen, Yazhou Yao, Tao Chen, Xian-Sheng Hua, and Heng-Tao Shen, “Hierarchical graph pattern understanding for zero-shot video object segmentation,” *IEEE Transactions on Image Processing*, vol. 32, pp. 5909–5920, 2023.
 - [19] Tao Chen, Yazhou Yao, and Jinhui Tang, “Multi-granularity denoising and bidirectional alignment for weakly supervised semantic segmentation,” *IEEE Transactions on Image Processing*, vol. 32, pp. 2960–2971, 2023.
 - [20] Tao Chen, Yazhou Yao, Xingguo Huang, Zechao Li, Liqiang Nie, and Jinhui Tang, “Spatial structure constraints for weakly supervised semantic segmentation,” *TIP*, vol. 33, pp. 1136–1148, 2024.
 - [21] Gensheng Pei, Tao Chen, Xiruo Jiang, Huafeng Liu, Zeren Sun, and Yazhou Yao, “Videomac: Video masked autoencoders meet convnets,” *CVPR*, pp. 22733–22743, 2024.
 - [22] Gensheng Pei, Yazhou Yao, Fumin Shen, Dan Huang, Xingguo Huang, and Heng-Tao Shen, “Hierarchical co-attention propagation network for zero-shot video object segmentation,” *IEEE Transactions on Image Processing*, vol. 32, pp. 2348–2359, 2023.
 - [23] Tao Chen, Yazhou Yao, Lei Zhang, Qiong Wang, Guosen Xie, and Fumin Shen, “Saliency guided inter- and intra-class relation constraints for weakly supervised semantic segmentation,” *IEEE Transactions on Multimedia*, vol. 25, pp. 1727–1737, 2023.
 - [24] Tao Chen, Guosen Xie, Yazhou Yao, Qiong Wang, Fumin Shen, Zhenmin Tang, and Jian Zhang, “Semantically meaningful class prototype learning for one-shot image segmentation,” *IEEE Transactions on Multimedia*, vol. 24, pp. 968–980, 2022.
 - [25] C. Zhang, L. Wang, S. Cheng, and Y. Li, “Swinsunet: Pure transformer network for remote sensing image change detection,” *IEEE Transactions on Geoscience and Remote Sensing*, vol. 60, pp. 1–13, 2022.
 - [26] H. Chen, Z. Qi, and Z. Shi, “Remote sensing image change detection with transformers,” *IEEE Transactions on Geoscience and Remote Sensing*, vol. 60, pp. 1–14, 2021.
 - [27] W. G. C. Bandara and V. M. Patel, “A transformer-based siamese network for change detection,” in *IEEE International Geoscience and Remote Sensing Symposium*, 2022, pp. 207–210.
 - [28] I. Radosavovic, R. P. Kosaraju, R. Girshick, K. He, and P. Dollár, “Designing network design spaces,” in *IEEE Conference on Computer Vision and Pattern Recognition*, 2020, pp. 10428–10436.
 - [29] S. Ji, S. Wei, and M. Lu, “Fully convolutional networks for multisource building extraction from an open aerial and satellite imagery data set,” *IEEE Transactions on Geoscience and Remote Sensing*, vol. 57, no. 1, pp. 574–586, 2018.
 - [30] H. Chen and Z. Shi, “A spatial-temporal attention-based method and a new dataset for remote sensing image change detection,” *Remote Sensing*, vol. 12, no. 10, pp. 1662, 2020.
 - [31] Q. Shi, M. Liu, S. Li, X. Liu, F. Wang, and L. Zhang, “A deeply supervised attention metric-based network and an open aerial image dataset for remote sensing change detection,” *IEEE Transactions on Geoscience and Remote Sensing*, vol. 60, pp. 1–16, 2021.
 - [32] C. Zhang, P. Yue, D. Tapete, L. Jiang, B. Shangguan, L. Huang, and G. Liu, “A deeply supervised image fusion network for change detection in high resolution bi-temporal remote sensing images,” *ISPRS Journal Of Photogrammetry And Remote Sensing*, vol. 166, pp. 183–200, 2020.
 - [33] S. Fang, K. Li, J. Shao, and Z. Li, “Snunet-cd: A densely connected siamese network for change detection of vhr images,” *IEEE Geoscience and Remote Sensing Letters*, vol. 19, pp. 1–5, 2021.
 - [34] A. Codegoni, G. Lombardi, and A. Ferrari, “Tinycd: a (not so) deep learning model for change detection,” *NEURAL COMPUTING & APPLICATIONS*, vol. 35, no. 11, pp. 8471–8486, 2023.
 - [35] L. Yan and J. Jiang, “A hybrid siamese network with spatiotemporal enhancement and two-level feature fusion for remote sensing image change detection,” *IEEE Transactions on Geoscience and Remote Sensing*, vol. 61, pp. 1–17, 2023.
 - [36] X. Tang, T. Zhang, J. Ma, X. Zhang, F. Liu, and L. Jiao, “Wnet: W-shaped hierarchical network for remote sensing image change detection,” *IEEE Transactions on Geoscience and Remote Sensing*, vol. 61, pp. 1–14, 2023.
 - [37] T. Yan, Z. Wan, P. Zhang, G. Cheng, and H. Lu, “Transy-net: Learning fully transformer networks for change detection of remote sensing images,” *IEEE Transactions on Geoscience and Remote Sensing*, vol. 61, pp. 1–12, 2023.
 - [38] E. Xie, W. Wang, Z. Yu, A. Anandkumar, J. M. Alvarez, and P. Luo, “Segformer: Simple and efficient design for semantic segmentation with transformers,” in *Conference and Workshop on Neural Information Processing Systems*, 2021, vol. 34, pp. 12077–12090.
 - [39] A. Paszke, S. Gross, F. Massa, A. Lerer, J. Bradbury, G. Chanan, T. Killeen, Z. Lin, N. Gimelshein, L. Antiga, A. Desmaison, A. Kopf, E. Yang, Z. DeVito, M. Raison, A. Tejani, S. Chilamkurthy, B. Steiner, L. Fang, J. Bai, and S. Chintala, “Pytorch: An imperative style, high-performance deep learning library,” in *Advances in Neural Information Processing Systems*, 2019, vol. 32, pp. 1–12.
 - [40] D. P. Kingma and J. Ba, “Adam: A method for stochastic optimization,” in *International Conference on Learning Representations*, 2015, pp. 1–15.